

# Resonance production of keV sterile neutrinos in core-collapse supernovae and lepton number diffusion

Vsevolod Syvolap,<sup>1,2</sup> Oleg Ruchayskiy,<sup>1</sup> and Alexey Boyarsky<sup>3</sup>

<sup>1</sup>*Discovery Center, Niels Bohr Institute, Copenhagen University, Blegdamsvej 17, Copenhagen, DK-2100, Denmark*

<sup>2</sup>*Taras Shevchenko National Technical University, Kiev, Ukraine*

<sup>3</sup>*Lorentz Institute, Leiden University, Niels Bohrweg 2, Leiden, NL-2333 CA, The Netherlands*

We investigate how hypothetical particles – sterile neutrinos – can be produced in the interior of exploding supernovae via the resonant conversion of  $\bar{\nu}_\mu$  and  $\bar{\nu}_\tau$ . The novelty of our treatment lies in the proper account of the resulting lepton number diffusion. We compute the yield of sterile neutrinos and find that even after taking into account back reaction, sterile neutrinos can carry out a sizeable fraction of the total energy of the explosion comparable to that of active neutrinos. The production is, however, exponentially sensitive to the temperature in the inner supernovae regions, making robust predictions of challenging. In order to understand whether this production affects supernova evolution and can therefore be constrained, detailed simulations including the effects of sterile neutrinos are needed.

## I. INTRODUCTION AND OUTLOOK

Exploding supernovae (SNe) are characterised by high temperatures  $T \sim \mathcal{O}(10)$  MeV and high densities of baryons. This makes them unique laboratories that can copiously produce hypothetical feebly interacting particles [1–3], including axions, dark photons, millicharged particles, sterile neutrinos (see *e.g.* [4, 5]).

SN medium is not transparent for neutrinos of all flavours, and their dispersion relations change, as compared to the vacuum case  $\omega = |k|$  [6]. In the models with *sterile neutrinos* ( $\nu_s$ ) – massive neutral particles, that mix with active neutrinos – this may lead to the enhancement of active-sterile mixing, similarly to the solar MSW effect [7, 8]. Feeble interaction of the resulting particles allows them to escape from the interiors of SNe.

The question of sterile neutrino production during supernovae explosion, their effects on explosion, and on the stellar nucleosynthesis has been studied in the past [9–28]. These studies mostly concentrated on the mixing of sterile neutrino with electron flavour, owing to the presence of the significant electron lepton number  $L_e$  in the supernova. The production of  $\nu_s$  from  $\mu$  and  $\tau$  flavours has been considered in [17, 24, 29].<sup>1</sup> These works took into account production via scattering in the constant-density core of the supernova, expecting that the effect should be the strongest there due to the high density of matter and temperature.

The question of production of  $\nu_s$ , mixed with  $\nu_x$  has been re-analysed recently in [30] where it had been noticed that outside the core the resonant MSW-like conversion of  $\bar{\nu}_x$  into sterile neutrino  $\nu_s$  was possible (see also [31]). It was argued in [30] that such a conversion can be quite efficient and can lead to a significant flux of  $\nu_s$  for mixing angles as small as  $\sin^2(2\theta_{\mu,\tau}) \sim 10^{-12}$ .

In this work we re-analyse sterile neutrino production in the course of supernovae explosion, taking into account back-reaction of sterile neutrino emission on the local density of anti-neutrinos. We demonstrate that – the local density of anti-neutrinos  $\bar{\nu}_x$  in the resonance zone is quickly reduced (the chemical potential  $\mu_x \gtrsim T$  is generated), thus slowing the sterile neutrino production. – The diffusion processes are not efficient enough to restore the population of  $\bar{\nu}_x$  in the resonance zone. – The exact amount of energy carried by sterile neutrinos is exponentially sensitive to the temperature in the inner SN regions. This makes robust predictions of sterile neutrino flux highly challenging, as these temperatures are not sufficiently constrained.

As a result the process of sterile neutrino production eventually switches off. Nevertheless we find that sterile neutrinos can carry out a significant fraction of the total energy of the explosion, comparable with the energy flux of a flavour of active neutrinos. *This constitutes the main result of our paper.*

The structure of the paper and the main points of each Section are as follows:

- Section II lists the formulas that are sufficient to reproduce our results and explains basic ingredients that enter the computations. Details and comments, accompanying these formulas are provided in Appendices
- Section III presents our results: we estimate the amount of energy carried away by  $\nu_s$ , calculate their spectra and evolution of the chemical potential of  $\mu$  and  $\tau$  flavours in space and time. **Our main results are summarised in Figs. 1.**
- In Section IV we conclude that although sterile neutrino production can be quite efficient, it is difficult to obtain robust constraints on sterile neutrino parameters based on the scarce data we have and that one needs holistic simulations of SN explosions, including sterile neutrinos in order to see whether too much energy gets carried away through this channel.

---

<sup>1</sup> In what follows we will use the notation  $\nu_x$  to denote collectively ( $\nu_\mu, \nu_\tau$ ) and  $\bar{\nu}_x$  for ( $\bar{\nu}_\mu, \bar{\nu}_\tau$ ) respectively.

- Appendices A–D provide background information and additional cross-checks; details of derivation of the kinetic equation; treatment of the diffusion, etc.

**Note added.** When this manuscript was finished, the paper [31] appeared that also investigates production of  $\nu_s$  mixed with  $\nu_\tau$  in the SN interior. Ref. [31] analyses the evolution of the lepton asymmetry  $Y_\tau$  due to the resonance conversion and the collisional production as well as the feedback on the effective potential. The work [31] treats neutrino propagation microscopically, tracking individual particles, while we are using a macroscopic approach describing the overall effects of back-reaction via evolution of a thermodynamic quantity – chemical potential. Our results are qualitatively similar, the differences can be attributed to different temperature models to which the overall production is highly sensitive.

## II. SKETCH OF THE COMPUTATIONS

In order to keep the presentation simple and spare readers from technical details, we start by summarising

$$\frac{d^2 N_s(t, E)}{dE d\Omega} = \int_0^t 4\pi R_{\text{res}}^2(E) E^2 \bar{f}_x^{\text{out}}(t', R_{\text{res}}(E), E) P_{x \rightarrow s}(E) e^{-R_{\text{fwhm}}/\lambda_{\text{mfp}}} dt'. \quad (1)$$

Expression (1) requires several comments.  $R_{\text{res}}(E)$  is the radius, at which resonance condition is satisfied for anti-neutrinos with the energy  $E$ . Relation  $r = R_{\text{res}}(E)$  can be inverted to form  $E = E_{\text{res}}(r)$  and determines the value of the energy of  $\nu_s$  produced at radius  $r$ :

$$E_{\text{res}}(r) = \frac{m_s^2}{V_{\text{eff}}(r)}. \quad (2)$$

$V_{\text{eff}}(r)$  is the *effective potential* of anti-neutrinos [6]. For the  $\bar{\nu}_\mu$ :

$$V_{\text{eff}}(r) = -\frac{G_F}{\sqrt{2}} N_b (Y_n - 2Y_{\nu_e} - 2Y_{\nu_\tau} - 4Y_{\nu_\mu} - 2Y_\mu) \quad (3)$$

Here  $Y_i \equiv \frac{N_i - N_{\bar{i}}}{N_b}$  is the asymmetry in  $i^{\text{th}}$  particle ( $i = \{n, p, e, \mu, \tau, \nu_e, \nu_\mu, \nu_\tau\}$ ),  $N_b$  is the baryons number density. All these quantities are functions of position, see App. A. The effective potential for  $\bar{\nu}_\tau$  is obtained by the replacement  $\mu \leftrightarrow \tau$  and  $\nu_\mu \leftrightarrow \nu_\tau$  in (3). The baryon density  $N_b$  and asymmetries reach their maximal values in the SN core. Therefore, the energy (1) has a minimal value and the spectrum of emitted sterile neutrinos is cut at low energies.

Initially,  $Y_{\nu_\mu} = Y_{\nu_\tau} = 0$ ,  $Y_n = 0.7$ , and  $Y_{\nu_e} \sim 0.1$ . Therefore the effective potential (3) is *negative*, meaning that indeed the resonance occurs for anti-neutrinos.

the main steps of our calculations and basic formulas that would allow one to reproduce our results. Details of the derivation and calculation are provided in the Appendix B below.

In order to compute the production of sterile neutrinos we need to solve a *system of coupled equations*

1. First equation (Eq. (1) below) describes the temporal evolution of the distribution function of sterile neutrinos, based on which one can compute, *e.g.*, sterile neutrino energy flux.
2. Second equation (Eq. (8) below) governs the evolution of the chemical potential  $\mu_x(r, t)$ , that describes the back-reaction of the sterile neutrino production on the population of active anti-neutrinos.

The number of  $\nu_s$  with energy  $E$ , resonantly produced by the time  $t$  and travelling into the solid angle  $d\Omega$  is given by (we assume that  $E \approx |\vec{p}|$ , *i.e.* sterile neutrinos are ultra-relativistic):

Probability of transition  $P_{x \rightarrow s}$  is defined as:

$$P_{x \rightarrow s} = 1 - \exp\left[-\frac{\pi^2}{2} \frac{R_{\text{fwhm}}}{L_{\text{osc}}}\right] \quad (4)$$

where  $R_{\text{fwhm}}$  is the width of the resonance region,

$$R_{\text{fwhm}} = \frac{2 \sin 2\theta_0}{\left|\frac{\partial \log V_{\text{eff}}^{\text{res}}}{\partial r}\right|}, \quad (5)$$

(derivative of  $V_{\text{eff}}$  is evaluated at  $r = R_{\text{res}}$ ) and  $L_{\text{osc}}$  is the oscillation length at the resonance

$$L_{\text{osc}} = \frac{2\pi}{|V_{\text{eff}}^{\text{res}}| \sin 2\theta_0}. \quad (6)$$

The angle  $\theta_0$  is the vacuum active-sterile neutrino mixing and all equations are derived for  $\theta_0 \ll 1$ .

The distribution function  $\bar{f}_x^{\text{out}}$  describes *outgoing* anti-neutrinos at the radius  $r = R_{\text{res}}(E)$ . This function has the *equilibrium* form

$$\bar{f}_x(t, r, E) = \frac{1}{(2\pi)^3} \frac{1}{\exp\left[\frac{E + \mu_x(r, t)}{T(r)}\right] + 1} \quad (7)$$

The evolution of the anti-neutrino population is fully encoded in the chemical potential  $\mu_x(r, t)$ , we do not take

into account temperature evolution during the first second of explosion.

Factor  $e^{-R_{\text{fwhm}}/\lambda_{\text{mfp}}}$  where  $\lambda_{\text{mfp}}$  is the mean free path of  $\bar{\nu}_x$  in the resonance region accounts for the *neutrino damping* [32], see Section III 4 below.

For the distribution (7) the relation between the chem-

ical potential and the asymmetry  $Y_x$  is defined as:

$$Y_x = \frac{1}{N_b} \left( \frac{\mu_x T^2}{6} + \frac{\mu_x^3}{6\pi^2} \right) \quad (8)$$

and the evolution of  $Y_x$  is given by

$$\frac{\partial Y_x(r, t)}{\partial t} = \frac{\pi}{6} G_F^2 r^2 N_b(r) \frac{\partial}{\partial r} \left( \frac{r^2}{N_b(r)} \frac{\partial \mu_x(r, t)}{\partial r} \right) + \frac{\pi}{N_b(r)} E_{\text{res}}^2(r, t) \bar{f}_x(E_{\text{res}}(r), r, t) P_{x \rightarrow s}(E_{\text{res}}(r), r, t) \frac{dE_{\text{res}}(r, t)}{dr}, \quad (9)$$

Core radius	$R_{\text{core}} = 10 \text{ km}$
Max. Temperature	$T_{\text{max}} = 30 \text{ MeV}$
Min. Temperature	$T_{\text{min}} = 3 \text{ MeV}$
Baryon core density	$\rho_0 = 3 \times 10^{14} \frac{\text{g}}{\text{cm}^3}$
Baryon core number density	$N_0 = 10^{38} \text{ cm}^{-3}$
Proton fraction	$Y_p = 0.3$

TABLE I. Parameters of the fiducial model of the supernova adopted in this work. Temperature is chosen to decrease linearly from  $T_{\text{max}}$  at  $r = 0$  to  $T_{\text{min}}$  at  $r = 50 \text{ km}$  and is also constant during the first second. See Appendix A for other details.

where the first term describes the diffusion of the lepton number and the second term – the change of lepton asymmetry due to the conversion of anti-neutrinos into  $\nu_s$ .

Taking into account an implicit dependence of  $E_{\text{res}}$  on  $\mu_x$ , we can solve (9) for  $\mu_x(r, t)$ , plug it into Eq. (1), and find the distribution function of sterile neutrinos  $N_s(E, t)$ .

### III. RESULTS

#### 1. Energy output in sterile neutrinos

The machinery sketched in Section II allows us to calculate the energy spectra and the total energy emitted in the form of sterile neutrinos  $\nu_s$  during the *first second* of the core bounce.<sup>2</sup> Our results are summarised in Fig. 1 (energy carried out as a function of sterile neutrino parameters). In order to reduce uncertainties associated with our modelling of SN, we express the energy output of sterile neutrinos as a multiple of  $E_{\bar{\nu}_\tau}^{(1\text{sec})}$  – energy, emitted in the same model in the form of anti-neutrinos  $\bar{\nu}_\tau$  during the same first second (which is a factor of  $\sim 2$  less

than the overall energy, carried out by  $\bar{\nu}_\tau$  during the SN explosion). Results for  $E_s = 3E_{\bar{\nu}_\tau}^{(1\text{sec})}$ ,  $E_s = 2E_{\bar{\nu}_\tau}^{(1\text{sec})}$  and  $E_s = E_{\bar{\nu}_\tau}^{(1\text{sec})}$  are shown in Fig. 1, left to right. Maximal energy that can be carried by sterile neutrinos in the fiducial model is  $\approx 5E_{\bar{\nu}_\tau}^{(1\text{sec})}$ .<sup>3</sup>

The amount of energy emitted by sterile neutrinos depends strongly on the assumed temperature. In Fig. 1 we also demonstrate how our results change under “reasonable” modifications of the SN temperature model: change of the maximal temperature (hatched regions) up to 5 MeV. This indicates a level of systematic uncertainty of our estimates, although by no means fully describes it. The minimal temperature at  $r = R_{\nu_{\text{sph}}}$  is kept the same ( $T_{\text{min}} = 3 \text{ MeV}$ ), in order not to affect emission of active neutrinos.

The strong dependence of the sterile neutrino output on the parameters of the SN model can be understood as follows. For masses  $m_s \gtrsim 10 \text{ keV}$  the resonance energy is *higher* than the temperature of active neutrinos at  $R_{\text{res}}$ , see Fig. A.1. As a result, the number of  $\bar{\nu}_x$  participating in resonance conversion is exponentially sensitive to the temperature of the resonance region.

*We stress that Figs. 1 do not correspond to any constraints on sterile neutrino parameters – given our current knowledge about the SN explosion, it is impossible to predict exactly how much energy has been carried away by sterile neutrinos and what energy loss would be incompatible with scarce observations of SN1987A (see Section IV for discussion).*

#### 2. The importance of diffusion

The solution of Eq. (9) allows to find the evolution of the chemical potential  $\mu_x$  that governs the distribution

<sup>2</sup> After  $\sim 1 \text{ sec}$  the temperature of the SN cannot be considered as constant anymore, it decreases and the production of sterile neutrinos is essentially switched off.

<sup>3</sup> Such a powerful production is not treated self-consistently – the assumption of constant temperature would not hold anymore in this case. The more detailed investigation, however, is beyond the scope of this paper.

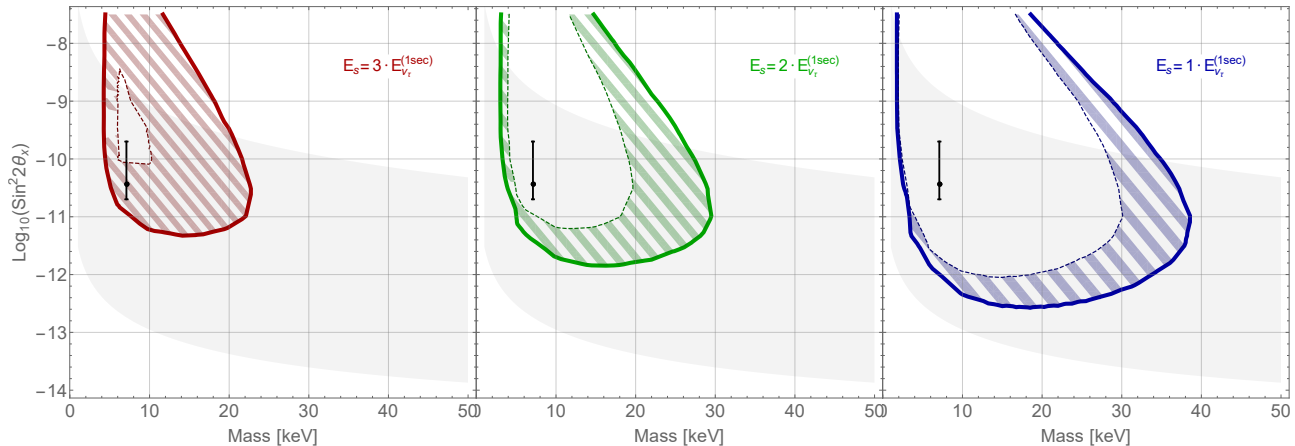


FIG. 1. **Main results:** Energy  $E_s$  carried out by sterile neutrinos, produced via resonant conversion from  $\bar{\nu}_\tau$  during the first second after the SN core bounce. Different panels show the values of the emitted sterile neutrino energy in multiples of  $E_{\bar{\nu}_\tau}^{(1\text{sec})}$  – energy carried away by  $\bar{\nu}_\tau$  during the same 1 sec (which is *less* than the total energy emitted in neutrinos of this type during the whole explosion). The plots demonstrate the uncertainty related to the SN temperature model. Colour solid lines show the results for our fiducial model (Table I). If the SN maximal temperature is *lowered* from  $T_{\text{max}} = 30$  MeV to  $T_{\text{max}} = 25$  MeV the curve sweeps the hatched region. Although our analysis did not assume that sterile neutrinos are dark matter particles, we overimpose light grey region to indicate where the correct dark matter abundance of sterile neutrinos can be generated in the *Neutrino Minimal Standard Model* ( $\nu\text{MSSM}$  see Section III 5). Black dot with error bars corresponds to the 3.5 keV signal of [33, 34] interpreted in terms of decays of sterile neutrino dark matter.

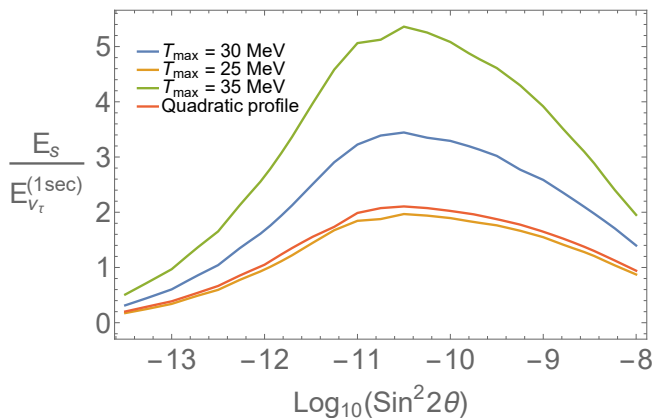


FIG. 2. Uncertainties related to the SN temperature models. Energy, emitted in the form of sterile neutrinos during the first second in multiples of  $E_{\bar{\nu}_\tau}^{(1\text{sec})}$  as a function of the mixing angle for the mass  $m_s = 20$  keV. The curves show the effects of changing the maximal temperature  $T_{\text{max}}$  by  $\pm 5$  MeV as well as and different scaling of the temperature profile between  $T_{\text{max}}$  and  $T_{\text{min}}$  (quadratic rather than linear).

of active anti-neutrinos. It is shown in Fig. 3. One sees that  $\mu_x/T$  can reach significant values ( $\mu_x \gtrsim T$ ).

To demonstrate the importance of back-reaction effects we also studied two extreme scenarios: (i) the absence of diffusion and (ii) the absence of back-reaction (infinite reservoir of neutrinos  $\bar{\nu}_x$  at every energy and radius).

In the former case the production  $\bar{\nu}_x \rightarrow \nu_s$  stops very quickly, as the resonant conversion “consumes” all active anti-neutrinos at a given radius and there are no mechanisms to replenish their population, as the large number of  $\nu_x$  prevents creation of  $\nu_x \bar{\nu}_x$  pairs via Pauli blocking. (see also Appendix D for more details). Therefore the sizeable production of sterile neutrinos is possible in this case only for sufficiently large values of the mixing angle. In the case (ii), the population of anti-neutrinos  $\bar{\nu}_x$  gets immediately restored and therefore the conversion rate remains the same through the whole time  $t_{\text{pb}} \sim 1$  sec, being extremely efficient. The production in the case (ii) stops only because neutrino sufficiently cool down with the SN. It is this approximation that was used in [30] which explains higher total energy emitted in sterile neutrinos in their case. The realistic back-reaction is in-between these two limiting cases, as Fig. 4 demonstrates.

The spectra of the resulting sterile neutrinos with different diffusion treatment are shown in Fig. 5.

### 3. Difference between muon and tau mixings

Although the presented mechanism works for both  $\mu$ - and  $\tau$ -mixing, the treatment of these two flavours differs, due to the fact that the temperature of the SN interior is high enough for muon pairs to be present (but not for tau leptons). As discussed in Appendix A generation of non-zero chemical potential of  $\nu_\mu$  affects the popula-

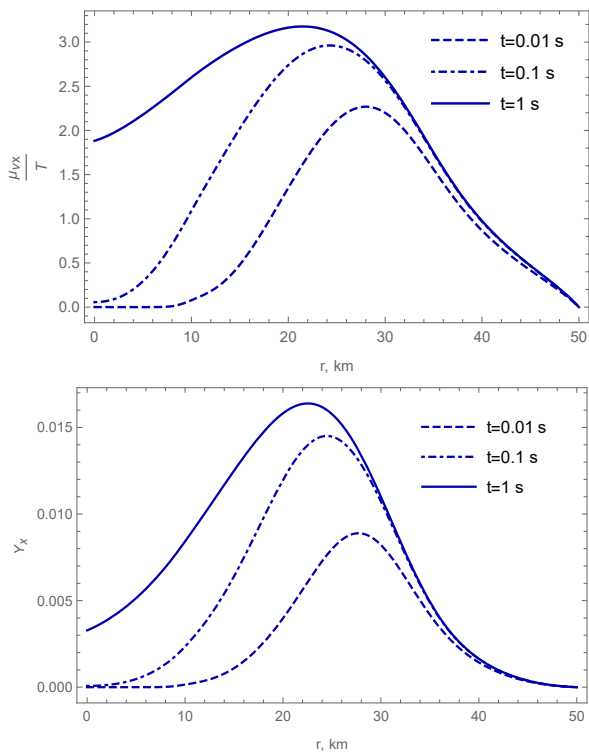


FIG. 3. Time evolution of the radial profiles of the chemical potential  $\mu_\tau$  and of the asymmetry parameter  $Y_\tau$  in the fiducial model. Parameters of sterile neutrino are: mass  $m_s = 7.1$  keV, the mixing angle  $\sin^2 2\theta_\tau = 5 \times 10^{-11}$ . The production of asymmetry starts at radii  $r = 20 - 30$  km, and then diffuses to the inner regions of the SN (recall that we consider the constant density NS core with  $R_{\text{core}} = 10$  km). At the same time, equilibrium between diffusion and production is achieved in the outer layers within a fraction of a second and is maintained afterwards. The asymmetry parameter  $Y_x$  always remains below values  $\sim \mathcal{O}(0.1)$  where  $V_{\text{eff}}$  would change significantly.

tion of  $\mu^\pm$ , which (through electro-neutrality condition) affects the number of electrons, electron neutrinos, etc. We estimate the difference, using an approximate treatment (presented in Appendix A) and show the results in Fig. 6. One can see that within the precision of our treatment there is no difference in the resulting amount of energy, carried by either flavour. We do not discuss here the influence of charged muons on the SN explosion [35].

#### 4. Damping

The neutrino damping [32] describes the probability that a neutrino would interact with the medium while propagating in the resonance region. This interaction will cause the wave function to collapse to a pure flavour state, and its resonance conversion will become impossible. One can ignore the damping whenever  $R_{\text{fwhm}} \ll \lambda_{\text{mfp}}$ . In the opposite limit the collisional production be-

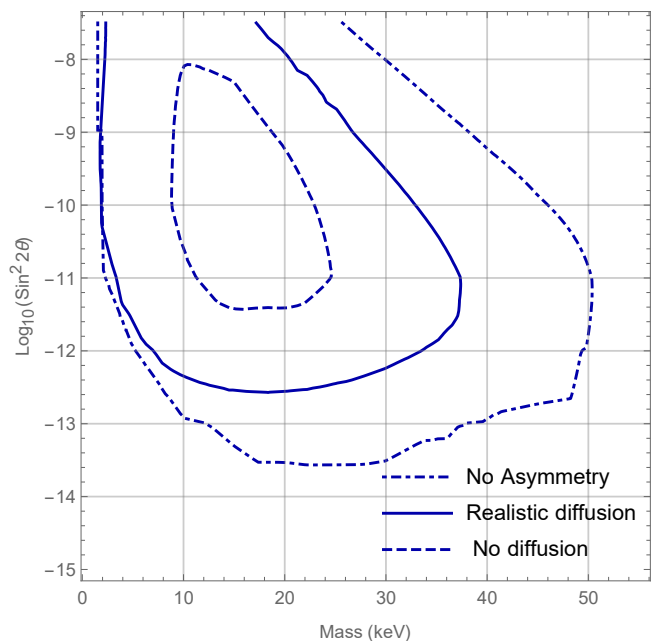


FIG. 4. Effects of the feedback. We show how one of the contours in Fig. 1 ( $E_s = E_{\nu_\tau}^{(1\text{sec})}$ ) changes for three different feedback mechanisms: the depleted lepton number is not repopulated by any means (“no diffusion” dashed line); the restoration of the lepton number proceeds much faster than sterile neutrino production (“no asymmetry” dashed-dotted line); and the case of the realistic diffusion, as studied in this work. The mixing is with  $\nu_\tau$  only and the duration of emission is taken to be 1 sec for all three cases. The SN fiducial model is given in Table I, uncertainties due to SN modelling are not shown.

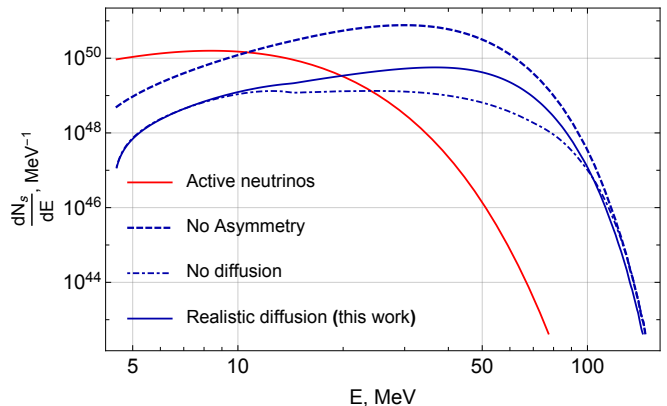


FIG. 5. Spectra of sterile neutrinos with mass  $m = 7.1$  keV and the mixing angle  $\sin^2 2\theta_x = 5 \times 10^{-11}$  produced during the first second of explosion for three cases of back reaction in the fiducial SN model (*cf.* Fig. 4). Sterile neutrinos are mixed with  $\tau$ -flavour. The spectrum of active neutrinos emitted during the same time (red solid line) is also shown for comparison. Active neutrinos are emitted from the radius  $R_{\nu_{\text{sph}}} > R_{\text{res}}$  and are therefore colder.

comes important, as the scattering has finite probability

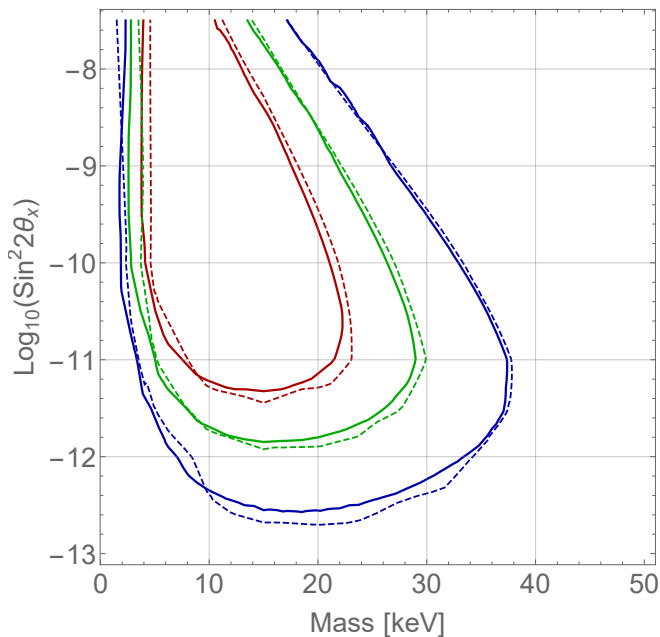


FIG. 6. Comparison between two cases: mixing with  $\bar{\nu}_\tau$  and mixing with  $\bar{\nu}_\mu$ . Unlike  $\tau$ -flavour asymmetry, muon lepton number may lead to a population of  $\mu^\pm$  in the SN interior. This affects electrons and electron neutrinos via electric neutrality and beta-equilibrium conditions and therefore changes the effectiveness of production. Only the results for the fiducial model are shown, it is clear that the differences are much below the uncertainties due to SN temperature modelling. Solid lines: mixing with  $\nu_\tau$ , dashed lines: mixing with  $\nu_\mu$ . *Blue lines*: contours where sterile neutrino energy release  $E_s = E_{\bar{\nu}_x}^{(1\text{sec})}$ , *green lines*:  $E_s = 2E_{\bar{\nu}_x}^{(1\text{sec})}$ , *red lines*:  $E_s = 3E_{\bar{\nu}_x}^{(1\text{sec})}$  (same colours as in Fig. 1).

to leave behind not only pure active but also pure sterile state. The collisional production have been considered before in many works (see *e.g.* [17, 24, 30, 31]) and it is beyond the scope of the current work to study how it combines with the resonant production.

The effects of neutrino damping are shown in Fig. 7. Its shape can be understood as follows: the width of the resonance  $R_{\text{fwhm}}$  is independent on the energy and proportional to the  $\sin(2\theta_0)$  (Eq. (5)) while the mean free path of active neutrinos scales with energy as  $E^{-2}$  (see Section C 2). As a result for a given mass  $m_s$  and position  $R_{\text{res}}$  (equivalently *fixed resonance energy*) the ratio  $R_{\text{fwhm}}/\lambda_{\text{mfp}}$  grows with  $\theta_0$ . If one keeps the mixing angle (and  $R_{\text{fwhm}}$ ) fixed, but rather increases the mass – the resonance energy is increasing (Eq. (2)). Therefore the mean free path of  $\bar{\nu}_x$  decreases and neutrino damping becomes important.

### 5. Sterile neutrino as dark matter

So far we did not make any reference to sterile neutrinos being dark matter particles. The lifetime of sterile

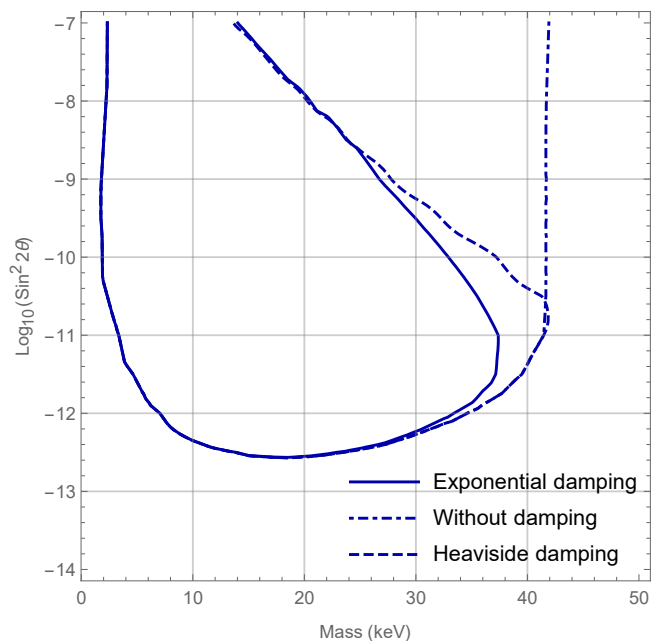


FIG. 7. Effects of neutrino damping on resonance production. The contours  $E_s = E_{\bar{\nu}_\tau}^{(1\text{sec})}$  are shown with and without damping effects included. If damping is not taken into account (dashed-dotted line) – the contour extends to higher masses and mixing angles. Dashed line represents neutrino damping treatment of [30] where condition  $R_{\text{fwhm}} \leq \lambda_{\text{mfp}}$  was imposed in Eq. (1) instead of the exponential function. In the region where the damping is noticeable the collisional production (not considered here) becomes important.

neutrinos lighter than two electron is given by (assuming for simplicity that  $\theta_x$  is the only non-negligible mixing)

$$\tau_s \approx 2 \times 10^{24} \text{ sec} \left( \frac{10^{-11}}{\sin^2(2\theta_x)} \right) \left( \frac{20 \text{ keV}}{m_s} \right)^5 \quad (10)$$

– much longer than the lifetime of the Universe when  $\theta^2 \sim 10^{-11}$ . And indeed such particles represent a viable dark matter candidate (as suggested in [15, 17, 36–38], see [39] for a review).

We compute the energy output for a sterile neutrino with mass  $m_s = 7.1 \text{ keV}$  and mixing angle  $\sin^2 2\theta_x = (2 - 20) \times 10^{-11}$ . Decay of such a sterile neutrino dark matter would produce an X-ray line, consistent with the observations of [33, 34] and many subsequent works, see [39] for details. In this case the energy output would be  $E_s \gtrsim 3 \times E_{\bar{\nu}_x}^{(1\text{sec})}$ , depending on the SN model assumed.

The grey shaded region in Fig. 1 shows the parameter space of the *Neutrino Minimal Standard Model* ( $\nu\text{MSM}$ ) [40, 41], see [42] for review where sterile neutrinos would have correct dark matter abundance (parts of this parameter space are excluded by X-ray and structure formation constraints, see [39] for review. The upper boundary corresponds to the parameters of the non-resonant dark matter production [17, 36, 38], while in the rest of the region the correct dark matter abundance can

be obtained in the presence of primordial lepton asymmetry [17, 37, 43]. The maximal value of lepton asymmetry required to produce the correct dark matter abundance depends on the ratio of the mixing angles and differs, for example, in the model where  $\theta_e = \theta_\mu = \theta_\tau$  as opposed to that with only  $\theta_\tau \neq 0$  [43, 44]. We conservatively chose to plot the lower bound corresponding to the maximal value of the lepton asymmetry attainable in the  $\nu$ MSM [43, 42].

#### IV. DISCUSSION

In this paper we analysed the process of sterile neutrino creation during the explosion of a core-collapse supernova. Sterile neutrinos are produced via mixing with active anti-neutrinos of  $\mu$  and/or  $\tau$  flavours (collectively,  $\bar{\nu}_x$ ). The hot and dense supernova environment is non-transparent for neutrinos and their dispersion changes as compared to the propagation in vacuum. Therefore, the mixing with sterile neutrinos can become *resonant* (the MSW-like effect), leading to the effective conversion of anti-neutrinos  $\bar{\nu}_x$  into sterile neutrinos with mass in the range  $5 \text{ keV} \lesssim m_s \lesssim 40 \text{ keV}$  and mixing angles  $\sin^2(2\theta_x)$  reaching  $10^{-8}$  and below. The question of sterile neutrino production during supernovae explosion, their effects on explosion, and on the stellar nucleosynthesis has been studied in the past for sterile neutrinos ranging in masses from eV to GeV [9–30, 45–47]. With few exceptions (*e.g.* [17, 24, 29, 30]) these studies concentrated on the mixings of sterile neutrino with electron flavour. Recent work [30] argued that the fast production of sterile neutrinos is possible due to the MSW-like resonance outside the SN core region when mixing with  $\bar{\nu}_x$ . However, the authors of [30] did not account for the depletion of the population of  $\bar{\nu}_x$  in the resonance region and kept the distribution of active anti-neutrinos at its equilibrium level, thus providing a “stock” of anti-neutrinos to be converted. In reality, the depletion of the active anti-neutrinos slows down the conversion process; the  $\nu_x - \bar{\nu}_x$  pair creation re-populates the abandoned states, and above-equilibrium excess of  $\nu_x$  gets diffused away.

In this work we properly took into account the diffusion of the lepton number and the back-reaction of sterile neutrinos on the neutrino distribution. Our results show that sterile neutrinos can carry away the amount of energy, comparable to that of active neutrino flavours (see Fig. 1). We can also recast our restrictions in terms of energy released during the explosion, Fig. 8. While the energy output can reach  $10^{53}$  ergs – a ballpark figure associated with a SN explosion – *this does not lead to the bounds that are both strong and robust.*

Indeed, two main types of bounds from supernovae exist: *energy loss* and *energy-loss rate* bounds, see *e.g.* [1–3, 48]. The emission of any exotic component can be capped from above by  $E_{\text{tot}}$  – the total energy available in explosion. The latter is the difference between the binding energies of a progenitor and a remnant. The estimates of the total released energy  $E_{\text{tot}}$  depend on

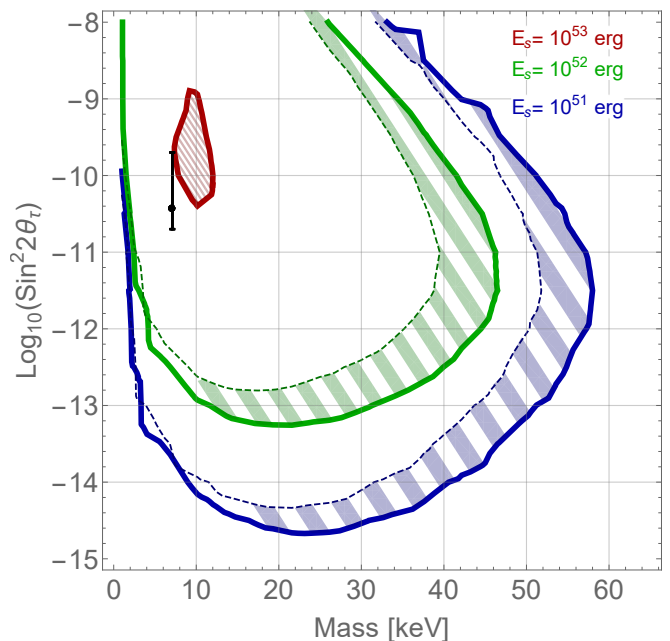


FIG. 8. Energy emitted by sterile neutrinos mixed solely with  $\nu_\tau$ . Assumptions are the same as in Fig. 1, but the results are expressed in ergs, rather than in fractions of  $E_{\bar{\nu}_\tau}^{(1\text{sec})}$ . This line corresponds to the parameters of the fiducial SN model, given in Table I. Shaded region indicates the level of uncertainty by showing how these contours change when the maximal temperature  $T_{\text{max}}$  is lowered from 30 MeV to 25 MeV. For comparison, the total energy emitted in *all active neutrino species during the 1st second* in our model is  $\sim 1.5 \times 10^{53}$  erg (and the total neutrino output over the whole duration of the collapse is about twice as much).

whether the remnant is a black hole or a neutron star. It is generally believed that the remnant of SN1987A is a neutron star, although the remnant has not been found [49] after more than 30 years of searches. The NS remnant can still be hidden behind SN debris [49, 50]. If the remnant is the neutron star, its binding energy can be estimated as

$$E_{\text{NS}} \approx 6.3 \times 10^{53} \text{ erg} \left( \frac{\mathcal{C}}{0.6} \right) \left( \frac{M_{\text{NS}}}{2M_\odot} \right)^2 \left( \frac{10 \text{ km}}{R_{\text{NS}}} \right) \quad (11)$$

with the coefficient  $\mathcal{C} \approx 0.6$  [51–53]. The estimates put the mass for the SN1987A remnant in the range  $M_{\text{NS}} \simeq 1.7 - 1.9M_\odot$ , see [49] for review. Alternative scenarios for a black hole formation in the SN1987A explosion exist [54–57]. In any case, the energy emitted in sterile neutrinos (Fig. 8) is much smaller than  $E_{\text{NS}}$ .

The energy loss rate argument applies to the particles, produced *in the NS core* [1–3]:  $\epsilon_{\text{extra}} \leq 10^{19} \text{ erg/sec/g}$  and is based on simulations, including emissions of new particles (axions in that case) [58–60]. Such a bound can be applied to sterile neutrinos, produce via scatterings [14, 17, 18, 23, 24]). However, in our case, *when new particles are produced only outside the core such bound can not be applied directly.*

In addition to the previous points, the output of sterile neutrinos is very sensitive to the temperature (and temperature profile) in the inner regions of the SN (Figs. 1 and 2). No observables are sensitive to the temperatures in these regions as the emission of active neutrinos happens from the outer regions – the neutrino-sphere with  $R_{\nu\text{sph}} > R_{\text{res}}$ . Therefore, even detailed measurements of the neutrino fluxes would not tell us about the conditions under which sterile neutrinos were produced. A knowledge of the temperature profile (that would allow to recover  $T(R_{\text{res}})$  given the “measurement” of  $T(R_{\nu\text{sph}})$ ) can only be inferred from the simulations (similar to *e.g.* [26, 28] that however deal with heavier sterile neutrinos and/or different production mechanisms and influence on the SN dynamics). Such bounds will necessarily be model-dependent. We live the self-consistent treatment of these cases to the future work.

Finally, we note that the same challenges are faced by energy loss bounds applied to other hypothetical very weakly interacting particles: axions, dark photons, millicharged particles, etc.

## ACKNOWLEDGEMENTS

We would like to thank G. Fuller, G. Raffelt, I. Tamborra, I. Timiryasov and Y.-Z. Qian for many useful discussions and comments on the draft. O.R. thanks the organisers of the “*Neutrino Quantum Kinetics in Dense Environments*” workshop for creating a stimulating environment. This work was supported by the Carlsberg foundation and by the European Research Council (ERC) under the European Union’s Horizon 2020 research and innovation programme (GA 694896).

## Appendix A: The supernova model

For our analytic description we used a SN model, that captures the effects of interest while is sufficiently simple to allow for analytic treatment. Namely, at times  $t_{\text{pb}} < 1$  sec after the core bounce we use static and uniform profiles for baryon, electron and electron neutrino densities inside the core. The baryon density is approximated as a constant inside the supernova core ( $r < R_{\text{core}}$ ) and decays exponentially at larger radii,

$$\rho_B = \rho_0 \exp\left[-\frac{r - R_{\text{core}}}{R_{\text{core}}}\right], \quad r > R_{\text{core}} \quad (\text{A.1})$$

Temperature is chosen to decrease linearly from  $T_{\text{max}}$  at  $r = 0$  to  $T_{\text{min}}$  at  $r = 50$  km and is also constant during the first second. Proton number fraction remains constant and it is just a simplification for our model (note that is not necessarily means that we define number of electrons as there may be change of population of other charge massive leptons). Along with baryon density, the conditions of charge neutrality and beta equilibrium define relations between densities of particles and their chemical potentials respectively:

$$\begin{aligned} Y_p &= Y_e + Y_\mu \\ \mu_e - \mu_{\nu_e} &= \mu_n - \mu_p = \hat{\mu} \\ \mu_\mu - \mu_{\nu_\mu} &= \mu_n - \mu_p = \hat{\mu} \end{aligned} \quad (\text{A.2})$$

Once the fraction of protons and neutrons is fixed, it defines  $\hat{\mu}$ , that shows the difference between the chemical potential of charged leptons and corresponding neutrino flavours. Any extra source of neutrino asymmetry will not affect baryons, leaving  $\hat{\mu}$  untouched, but will cause change in population of charged leptons (which can be neglected for tau-flavour due to  $\tau$  mass).<sup>4</sup> With sterile neutrinos, we will need equation of  $x$ -flavour neutrinos evolution, and it will totally define population of particles in media in our model.

Numerical values of the relevant parameters are specified in Table I.

At times  $t_{\text{pb}} > 1$  sec, temperature decreases to values below 5 MeV, which results in a low rate of  $\nu_s$  creation after the first second. That is why we do not take into account times  $t > 1$  sec.

### 1. Active neutrino energy output

While neutrinos are near the supernova core, they are trapped (i.e. the mean free path is small) and diffusion causes them to propagate to outer layers of the star. Starting from a particular radius, *transport neutrino-sphere radius*  $R_{\nu\text{sph}}$  the outgoing neutrinos freely escape from the supernova ( $\lambda_{\text{mfp}} \rightarrow \infty$ ).

$$R_{\nu\text{sph}}(E) = R_{\text{core}} \left(1 + \log(R_{\text{core}} \sigma(E) N_0)\right) \quad (\text{A.3})$$

<sup>4</sup> This effect, is small, see Figs. 6.

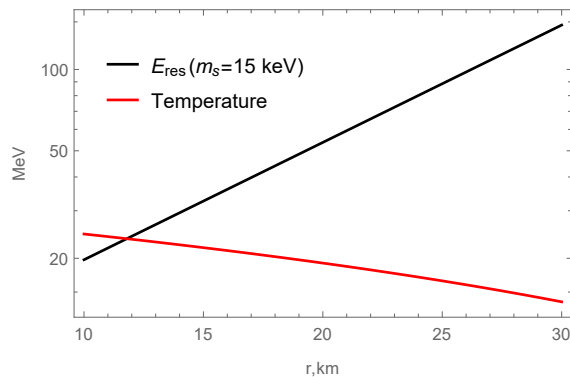


FIG. A.1. Temperature and resonance energy dependence on radius for sterile neutrino with mass  $m_s = 15$  keV. Resonance energy is almost everywhere higher than temperature, which means, population of neutrinos with given energy will be exponentially sensitive to choice of temperature. That explains high sensitivity of our main result to SN parameters choice.

Neutrinos that are emitted at  $r > R_{\nu\text{sph}}$  freely leave the star. Energy flux of  $\nu_x$  (or of  $\bar{\nu}_x$ ) per flavour is determined by

$$\frac{dQ}{dt dE d\Omega} = 4\pi R_{\nu\text{sph}}^2(E) E^3 f_x^{\text{out}} \quad (\text{A.4})$$

Integrating (A.4) over time and momentum gives energy, carried by one anti-neutrino species  $\bar{\nu}_x$  during the first second:  $E_{\bar{\nu}_x} \approx 2.2 \times 10^{52}$  erg. This value is close to the numerical result [53]  $(2.5 - 2.8) \times 10^{52}$  erg per neutrino species, which shows that our adopted SN model is realistic.

## Appendix B: Resonant sterile neutrinos production

For completeness we reproduce the formalism of the resonant conversion for neutrinos propagating in the media with changing density. Each of the flavour states  $\nu_x, \bar{\nu}_x$  as well as  $\nu_s$  obeys the Dirac equation and as a consequence the Klein-Gordon equation. When particles are ultra-relativistic in the medium of variable density this equation can be brought into the form (see *e.g.* the book [2, Chap. 8]):

$$i \frac{d}{dr} \begin{pmatrix} \bar{\nu}_x \\ \nu_s \end{pmatrix} = \mathcal{H}_{\text{eff}}(r) \begin{pmatrix} \bar{\nu}_x \\ \nu_s \end{pmatrix} \quad (\text{B.1})$$

where the “effective Hamiltonian” is

$$\mathcal{H}_{\text{eff}}(r) = \frac{m_s^2}{4E} \begin{pmatrix} -\cos 2\theta_0 & \sin 2\theta_0 \\ \sin 2\theta_0 & \cos 2\theta_0 \end{pmatrix} + \begin{pmatrix} V_{\text{eff}}(r) & 0 \\ 0 & 0 \end{pmatrix}. \quad (\text{B.2})$$

Here  $V_{\text{eff}}$  is the effective potential of  $\bar{\nu}_x$  given by (see Eq. (3) for details/notations):

$$V_{\text{eff}}(r) = -\frac{G_F}{\sqrt{2}} N_b (Y_n - 2Y_{\nu_e} - 2Y_{\nu_\tau} - 4Y_{\nu_\mu} - 2Y_\mu) = 11.4 \text{ eV} \left( \frac{N_b}{N_0} \right) (Y_n - 2Y_{\nu_e} - 2Y_{\nu_\tau} - 4Y_{\nu_\mu} - 2Y_\mu), \quad (\text{B.3})$$

$m_s$  is the mass of sterile neutrino,  $E$  is its energy ( $m_s \ll E$ ) and we have neglected masses of the active neutrinos;  $\theta_0$  is the vacuum active-sterile mixing angle. The sign of  $V_{\text{eff}}$  is such that only the mixing  $\bar{\nu}_x - \nu_s$  is relevant and therefore we have omitted  $\nu_x$  state in Eq. (B.1).

For future convenience we will introduce the notation

$$\Delta_s = \frac{m_s^2}{2E} \quad (\text{B.4})$$

When  $V_{\text{eff}} = 0$  the eigenvalues of the Hamiltonian (B.2) are  $\pm \frac{1}{2} \Delta_s$  and the vacuum active-sterile oscillation length is given by  $\pi / \Delta_s$ .

Notice that  $[\mathcal{H}_{\text{eff}}(r), \mathcal{H}_{\text{eff}}(r')] \neq 0$  for  $\theta_0 \neq 0$  and therefore exact solution of Eq. (B.1) is complicated. For the propagation inside the star where  $|\nabla \log V_{\text{eff}}| \ll \Delta_s$  one can, however, solve this equation in the adiabatic limit. To this end one diagonalizes (B.2) at every point by the matrix  $U(r)$ , given by

$$U(r) = \begin{pmatrix} \cos \theta(r) & \sin \theta(r) \\ -\sin \theta(r) & \cos \theta(r) \end{pmatrix} \quad (\text{B.5})$$

where the *matter mixing angle*  $\theta(r)$  is defined (assuming  $\theta_0 \ll 1$ )

$$\tan 2\theta(r) \simeq 2\theta_0 \frac{\Delta_s}{\Delta_s + V_{\text{eff}}(r)} + \mathcal{O}(\theta_0^2) \quad (\text{B.6})$$

From Eq. (B.6) one sees that deep inside the SN, where  $\Delta_s < |V_{\text{eff}}(r_{\text{in}})|$  and  $V_{\text{eff}} < 0$ , one has  $\tan 2\theta_{\text{in}} \rightarrow -0 \Leftrightarrow \theta_{\text{in}} \rightarrow \frac{\pi}{2}$ , because  $\theta$  is confined to  $0 \leq \theta \leq \frac{\pi}{2}$ . On the other hand, when the condition

$$\Delta_s + V_{\text{eff}}(r) = 0 \quad (\text{B.7})$$

is satisfied, one has a resonance and  $\theta_{\text{res}} \rightarrow \frac{\pi}{4}$ . Due to the sign of effective potential, resonance condition (B.7) can be satisfied only for anti-neutrinos. Eq. (B.7) establishes a relation between the anti-neutrino energy and the radius of the resonance,  $R_{\text{res}}$ :

$$V_{\text{eff}}(R_{\text{res}}) = -\frac{m_s^2}{2E} \quad (\text{B.8})$$

which leads to Eq. (2).

Diagonalisation of the Hamiltonian (B.2) gives two eigenvalues  $E_{a,b}(r)$  such that

$$E_{a,b}(r) = \frac{V_{\text{eff}}}{2} \pm \sqrt{(\Delta_s + V_{\text{eff}})^2 + 4\Delta_s^2\theta_0^2} \quad (\text{B.9})$$

and two eigenfunctions (mass eigenstates)  $\nu_{a,b}$ . In the medium with variable density the states  $\nu_{a,b}$  propagate according to the equation, similar to Eq. (B.1):

$$i \frac{d}{dr} \begin{pmatrix} \nu_a \\ \nu_b \end{pmatrix} = \begin{pmatrix} E_a(r) & i\theta'(r) \\ -i\theta'(r) & E_b(r) \end{pmatrix} \begin{pmatrix} \nu_a \\ \nu_b \end{pmatrix} \quad (\text{B.10})$$

The off-diagonal elements in the r.h.s. are equal to  $-iU^\dagger \partial_r U$  and are responsible for transition between different mass eigenstates that would be absent for  $\theta' = 0$ . Let us introduce a parameter of non-adiabaticity,  $\gamma$

$$\gamma \equiv \frac{\theta'(r)}{E_a(r) - E_b(r)} \quad (\text{B.11})$$

Its value determines whether a transition between different levels is possible. When  $\gamma \rightarrow 0$ , the evolution is fully adiabatic and transitions between mass eigenstates are negligible (this is the case, for example, in the Sun). It turns out that for small  $\theta_0$   $\gamma$  can be different from zero only in a narrow region around the resonance for a wide range of densities (effective potential) profiles (see Fig. B.1). This is the region where the mixing angle changes its value significantly. Defining this region as where  $\theta(r)$  changes from  $\sin^2 2\theta = 1$  to  $\sin^2 2\theta = \frac{1}{2}$  (*i.e.*  $\frac{\pi}{8} \leq \theta(r) \leq \frac{3\pi}{8}$ ) we get its width  $R_{\text{fwhm}} = 2 \sin(2\theta_0) / (\log V_{\text{eff}}(R_{\text{res}}))'$ , Eq. (5). The non-adiabaticity parameter is maximal at the resonance and can be expressed through the width of the resonance

$$\gamma = \frac{1}{\pi} \frac{L_{\text{osc}}}{R_{\text{fwhm}}} \quad (\text{B.12})$$

where  $L_{\text{osc}}$  is the oscillation length at resonance (6). The probability of transition between mass states  $\nu_a$  and  $\nu_b$  after crossing the resonance is given by [61]

$$P_{x \rightarrow s} = \frac{1}{2} - \left( \frac{1}{2} - P_{\text{na}} \right) \cos 2\theta_{\text{in}} \cos 2\theta_{\text{out}} \quad (\text{B.13})$$

where  $\theta_{\text{in}} \simeq \frac{\pi}{2}$  – mixing angle, at the point of neutrino state creation and  $\theta_{\text{out}} = \theta(r_{\text{out}}) \simeq \theta_0$  – the vacuum mixing angle.  $P_{\text{na}}$  is a probability of transition between mass eigenstates due to non-adiabatic change of  $V_{\text{eff}}$ . In the case,

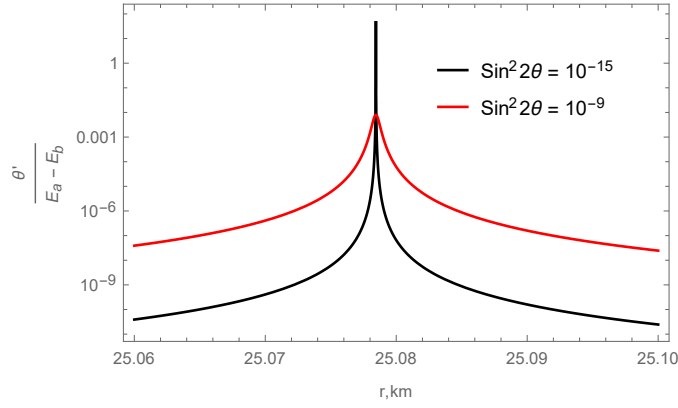


FIG. B.1. Evolution with radius of the adiabaticity parameter  $\gamma = \frac{\theta'}{E_a - E_b}$  (Eq. (B.11)). It can reach large values in a very narrow region around the resonance ( $R_{\text{res}} \simeq 25.078$  km in this case) and is extremely small outside it. The energy of the neutrino equals  $E = 40$  MeV, sterile neutrino mass  $m_s = 10$  keV. For smaller angle, the value of this parameter can be larger than 1. It shows that conversion goes non-adiabatically while for larger angle it acquires value  $\ll 1$  everywhere, so the conversion is totally adiabatic

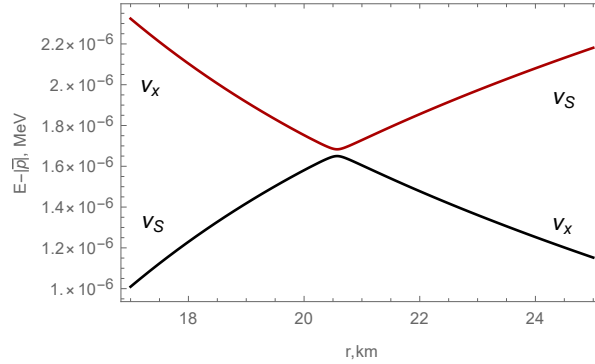


FIG. B.2. Energy levels  $E_a$  (black),  $E_b$  (red) of the system, depending on the radius. Mixing angle is chosen as  $\sin^2 2\theta = 10^{-3}$ , mass  $m_s = 10$  keV, momentum  $p = 30$  MeV. The  $y$ -axis shows  $m_{a,b}/2E$ . The closest distance between energy levels is at the resonance where the transition between the levels is the most likely.

when  $R_{\text{fwhm}}$  is much smaller than the characteristic scale, over which  $V_{\text{eff}}$  is changing, the effective potential can be approximated as a linear function of  $(r - R_{\text{res}})$  around the resonance. In this case the Landau-Zener formula appears

$$P_{\text{na}} = \exp\left[-\frac{\pi}{2\gamma}\right]. \quad (\text{B.14})$$

For small vacuum mixing angles one has  $\theta_{\text{in}} \approx \frac{\pi}{2}$  and  $\theta_{\text{out}} \approx \theta_0 \ll 1$ , Eq. (B.13) can be rewritten as

$$P_{x \rightarrow s} = 1 - \exp\left[-\frac{\pi}{2\gamma}\right]. \quad (\text{B.15})$$

Figure B.2 illustrates the above considerations. Energy levels  $E_a(r)$  and  $E_b(r)$  do not cross. The value  $E_a - E_b$  reaches its minimum as  $r \rightarrow R_{\text{res}}$ . In the case of fully adiabatic propagation (*i.e.* change of the radius) one remains on the same energy level  $E_a(r)$  or  $E_b(r)$ . As a result, a state  $|\nu_x\rangle$  that is *mostly*  $|\nu_a\rangle$  deep inside the star would remain *mostly*  $|\nu_a\rangle$  everywhere and would exit the star as mostly sterile state  $|\nu_s\rangle$ . The probability of such a process for  $\theta_0 \ll 1$  is given by  $P_{x \rightarrow s}^{\text{adiab}} \sim \cos^2 \theta_0 \rightarrow 1$  – the result familiar from the MSW effect in the Sun. This can be seen from Eq. (B.15) when the parameter of non-adiabaticity  $\gamma \rightarrow 0$ .

The non-diagonal elements in the Hamiltonian make propagation non-adiabatic. Therefore, although levels do not cross, when they are approaching close to each other, a transition between them can occur. As a result, the probability for an active neutrino to pass a resonance region without conversion remains finite. One can consider the limit  $\gamma \gg 1$ , where the probability behaves as  $P_{x \rightarrow s} \approx \frac{\pi}{2\gamma} = \frac{\pi^2}{2} \frac{R_{\text{fwhm}}}{L_{\text{osc}}} \ll 1$ .

## 1. Mixing with the electron flavour

The described mechanism can of course be used for  $\nu_e - \nu_s$  mixing as considered in a number of papers [9, 12, 45, 46]. The effective potential for  $\nu_e/\bar{\nu}_e$  is, however, different from (3):

$$V_{\text{eff}}^{\nu_e, \bar{\nu}_e}(r) = \mp \frac{G_F}{\sqrt{2}} N_b \left( -2Y_e + Y_n - 4Y_{\nu_e} - 2Y_{\nu_\tau} - 2Y_{\nu_\mu} \right). \quad (\text{B.16})$$

(the upper sign is for  $\nu_e$ , the lower  $-$  for  $\bar{\nu}_e$ ). Using the relations (A.2) one can see that the effective potential (B.16) changes its sign as one moves away from the core. As a result, the production is possible for both electron neutrinos and antineutrinos. While the resonant conversion for  $\bar{\nu}_e$  proceeds similarly to  $\bar{\nu}_x$ , for electron neutrinos the resonance condition is satisfied at two different radii. So  $\nu_s$  converted at an inner radius can be re-converted to active neutrinos at an outer radius, reducing the effectiveness of the production (see e.g. [45, Fig. 3]). The kinetic equation (1) does not take this into account. Another important effect is that the value of  $Y_{\nu_e}$  is tightly connected with the electron-positron asymmetry  $Y_e$  via beta-equilibrium condition. Therefore, efficient resonant conversion may shift beta-equilibrium and in this was significantly affect the nucleosynthesis in supernovae (see [62]). A proper self-consistent treatment of these processes are beyond the scope of this paper, therefore, we limit ourselves only to the mixing with  $\mu$  and  $\tau$  flavours.

## Appendix C: Back-reaction of sterile neutrinos

### 1. Evolution of $x$ -flavour population

The active-sterile conversion depletes the number of anti-neutrinos of a given energy at a given radius (the two are related via Eq. (2)). Therefore, the conversion could have led to the deviation of the  $\bar{\nu}_x$  distribution function from its initial equilibrium form. However, other processes such as nucleon-neutrino scatterings

$$\bar{\nu}_x + N \rightarrow \bar{\nu}_x + N \quad (\text{C.1})$$

lead to the change of the shape of the anti-neutrino distribution function without changing the total number of anti-neutrinos at the radius  $r$ . The nucleon-nucleon bremsstrahlung production of neutrino pairs,

$$N + N \rightarrow N + N + \bar{\nu}_x + \nu_x, \quad (\text{C.2})$$

partially re-populates the number of  $\bar{\nu}_x$  (without changing the total lepton number). The process (C.2) is stopped by the *neutrino* Pauli blocking. The reaction rates of the processes (C.1)–(C.2) are faster than sterile neutrino conversion rate [63]. Therefore we can always describe the population of  $\bar{\nu}_x$  by the equilibrium distribution function,

$$\bar{f}_x(E, r, t) = \frac{1}{(2\pi)^3} \frac{1}{\exp\left[\frac{E + \mu_x(r, t)}{T(r)}\right] + 1} \quad (\text{C.3})$$

(with  $\mu_x \rightarrow -\mu_x$  for neutrino distribution function). *The evolution of the neutrino population is fully encoded into the evolution of the chemical potential  $\mu_x$ .*<sup>5</sup>

The evolution of the chemical potential affects the effective potential  $V_{\text{eff}}$  and, therefore, the resonance energy (2) via the change of the lepton number  $Y_x$ . It can be seen from (2) that with the growth of  $Y_x$  the resonance energy increases, so that the number density of active anti-neutrinos with energy  $E \geq E_{\text{res}}$  diminishes and as a result the production stops.<sup>6</sup>

The non-zero chemical potential  $\mu_x \sim T$  means that neutrino average energy increases. For the muon flavour large values of  $\mu_x(r, t)$ , increase the number of neutrinos that can participate in the production of muons in reactions, like

$$\nu_\mu + n \rightarrow p + \mu^- \quad (\text{C.4})$$

$$\nu_\mu + e^- \rightarrow \mu^- + \nu_e \quad (\text{C.5})$$

$$\nu_\mu + \bar{\nu}_e \rightarrow \mu^- + e^+ \quad (\text{C.6})$$

<sup>5</sup> Recall that we only analyse the duration of time  $t_{\text{pb}} \sim 1$  sec and therefore neglect temporal change of the temperature profile.

<sup>6</sup> Sufficiently large asymmetry could cause the effective potential

to change the sign and therefore cause conversion  $\nu_x \rightarrow \nu_s$ . Such a process would result in washing out of the asymmetry. We will see below that this does not happen for the realistic values of the parameters.

leading to the non-negligible population of  $\mu^-$ . Similar reactions are possible for anti-neutrinos and anti-muons, but the number density of  $\bar{\nu}_\mu$  is extremely small in this regime, leading to negligible production of  $\mu^+$ . So the muon lepton asymmetry will be stored not only in neutrinos, but in muons as well. The population of  $\tau^\pm$  leptons remains negligible for because of their large mass.

## 2. Diffusion

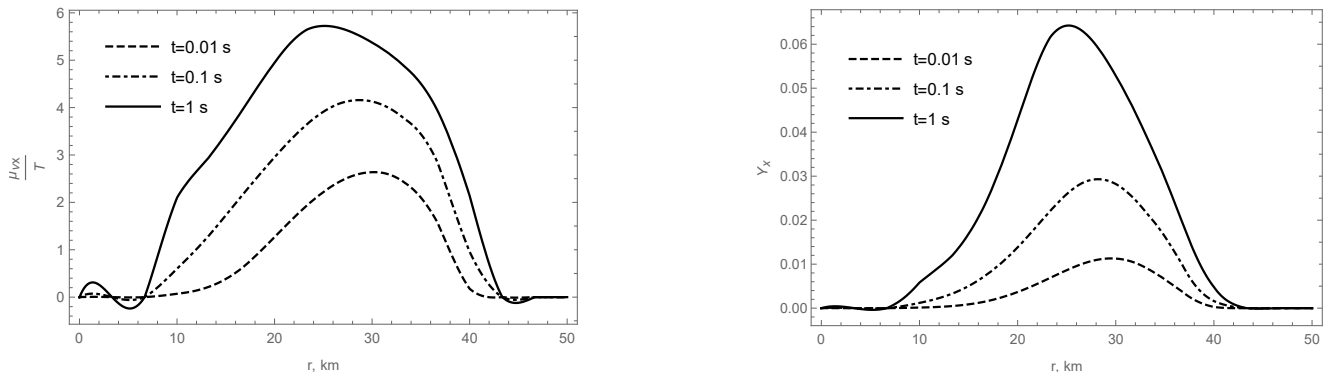


FIG. C.1. The same as for Fig. 3, but without diffusion. In this case asymmetry increases at every point independently. In the absence of diffusion the maximum asymmetry is sufficiently larger, but  $V_{\text{eff}}$  still does not changes sign. The peak position is changing slightly due to the change of resonance condition eq. (2) with the build up of the asymmetry  $Y$ . The non-zero values of  $\mu_x$  at radii  $r < 10$  km are numerical artifacts as there can be no resonant production in the constant density core region.

The inhomogeneous chemical potential  $\mu_x(r, t)$  triggers the lepton number diffusion processes. *Neutrinos* (whose number exceeds greatly that of anti-neutrinos) diffuse away and the reactions like (C.2) then replenish population of anti-neutrinos

A typical time scale for the diffusion over the distance  $R$  is  $t_{\text{Diff}} = \frac{R^2}{\lambda_{\text{mfp}}}$ , where  $\lambda_{\text{mfp}}$  is the mean free path of (anti)neutrinos of  $x$ -flavour. The neutrino mean free path depends on the neutrino energy and matter density. A straightforward computation of neutrino scattering in a medium of non-relativistic nucleons gives  $\lambda_{\text{mfp}} \sim \frac{\pi}{G_F^2 N_b E^2}$ .<sup>7</sup> Typical values of neutrino energies in supernovae is  $E \sim \mathcal{O}(100)$  MeV and densities can reach  $N_b \sim 2 \times 10^{38} \text{ cm}^{-3}$  so diffusion time can be as low as  $\mathcal{O}(10^{-2} \text{ sec})$  – much below the period of time over which we analyse the sterile neutrino production. Therefore diffusion cannot be neglected.

To describe the evolution of the lepton asymmetry we use (??) (Appendix D) with diffusion coefficient  $D(r, E)$  in the relaxation time-approximation:

$$D(r, E) = \frac{\lambda_{\text{mfp}}(r, E)}{3} = \frac{\pi}{3G_F^2 N_b(r) E^2} \quad (\text{C.7})$$

The collisional production of sterile neutrinos can also affect the evolution of the chemical potential. Indeed, let  $\Gamma_{\nu_x \rightarrow \nu_s}^{\text{coll}}$  be the rate of collisional production of sterile neutrinos  $\nu_x \rightarrow \nu_s$ , while  $\Gamma_{\bar{\nu}_x \rightarrow \nu_s}^{\text{coll}}$  be a similar rate for anti-neutrino production (of course,  $\nu_x$  and  $\bar{\nu}_x$  produce sterile states of opposite helicity). Naively, one could argue that as there are more  $\nu_x$  than  $\bar{\nu}_x$  in the resonance region, the collisions will predominantly convert  $\nu_x \rightarrow \nu_s$ , thus decreasing the asymmetry. This is, however, not the case as the collision rates are not the same,  $\Gamma_{\nu_x \rightarrow \nu_s}^{\text{coll}} \ll \Gamma_{\bar{\nu}_x \rightarrow \nu_s}^{\text{coll}}$  in the resonance region, see *e.g.* [17] where the resonance enhancement/suppression of the collisional production rate is discussed. Indeed, the collision rates are proportional to  $\sin^2(2\theta)$ . In the resonance region, angle for anti-neutrinos is  $\theta_{\text{res}}^{\bar{\nu}_x} \sim \mathcal{O}(1)$ , while for neutrinos  $\theta_{\text{res}}^{\nu_x} \simeq \frac{1}{2}\theta_0$ , as one can see by replacing  $V_{\text{eff}} \rightarrow -V_{\text{eff}}$  in Eq. (B.6) and making use of the condition (B.7). As a result

$$\Gamma_{\nu_x \rightarrow \nu_s}^{\text{coll}} \sim \theta_0^2 \Gamma_{\bar{\nu}_x \rightarrow \nu_s}^{\text{coll}} \quad (\text{C.8})$$

With chemical potential reaching  $\mu_x/T \sim 3$  (see Fig. 3)  $n_{\bar{\nu}_x} \sim 10^{-2} n_{\nu_x}$  and therefore we conclude that collisions do not contribute significantly to the wash out of lepton asymmetry for mixing angles that we are considering.

<sup>7</sup> Recall that we are interested only in the diffusion of  $\mu$  or  $\tau$  flavours and therefore only neutral current processes contribute

to the scattering of both neutrinos and anti-neutrinos.

### 3. Effects on the electron flavour population

As mentioned before, in the case of the mixing with  $\nu_\mu$ , development of the chemical potential of the muon lepton number would lead to the asymmetry in charged muons. This in turn will affect electrons and electron neutrinos via the charge neutrality condition  $Y_p = Y_e + Y_\mu$ , changing the asymmetry of electrons. Connection between charged leptons and correspondent neutrinos is expressed with beta-equilibrium relations:

$$\mu_\mu - \mu_{\nu_\mu} = \mu_n - \mu_p = \hat{\mu} \quad (\text{C.9})$$

$$\mu_e - \mu_{\nu_e} = \mu_n - \mu_p = \hat{\mu} \quad (\text{C.10})$$

Charge neutrality and beta-equilibrium allows us to connect all these parameters of the supernovae medium. As a consequence of the increase of the muon neutrino chemical potential, we will have decreased values of electron's density and density of  $\nu_e$ . This effect, however, affects the overall results only marginally, as the comparison between the mixings with  $\nu_\mu$  and  $\nu_\tau$  shows, see Figs. 6.

#### Appendix D: Lepton asymmetry evolution

We start from radial diffusion equation for distribution function with a source

$$\frac{\partial f_x(r, E, t)}{\partial t} = \frac{1}{r^2} \frac{\partial}{\partial r} \left( r^2 D(r, E) \frac{\partial f_x(r, E, t)}{\partial r} \right) + I_x(r, E, t) \quad (\text{D.1})$$

where  $f_x$  - distribution function of  $\nu_x$  ( $\bar{\nu}_x$ ),  $D(E, r)$  - diffusion coefficient,  $I_x(r, E, t)$  - source. By taking Eq. (D.1) for neutrinos and anti-neutrinos, integrating their difference over momentum, and dividing by  $N_b$  we find:

$$\frac{\partial Y_x(r, t)}{\partial t} = \frac{1}{N_b(r)} \frac{1}{r^2} \int \frac{\partial}{\partial r} \left( r^2 D(r, E) \frac{\partial}{\partial r} (f_x(E, r, t) - \bar{f}_x(E, r, t)) \right) d^3p + S_x(r, t) \quad (\text{D.2})$$

here  $S_x(r, t)$  is the integrated source of asymmetry

$$S_x(r, t) = \frac{\pi}{N_b(r)} E_{\text{res}}^2(r, t) f_x^{\text{out}}(E_{\text{res}}(r), r, t) P_{x \rightarrow s}(E_{\text{res}}(r), r, t) \frac{dE_{\text{res}}}{dr}(r, t) \quad (\text{D.3})$$

Combining these results together, we arrive to the final equation describing the evolution of lepton number, Eq. (9).

- 
- [1] G. G. Raffelt, Phys. Rept. **198**, 1 (1990).
  - [2] G. G. Raffelt, *Stars as laboratories for fundamental physics* (Chicago, USA: Univ. Pr. (1996) 664 p, 1996).
  - [3] G. G. Raffelt, Ann. Rev. Nucl. Part. Sci. **49**, 163 (1999), arXiv:hep-ph/9903472 [hep-ph].
  - [4] R. Essig *et al.*, in *Proceedings, 2013 Community Summer Study on the Future of U.S. Particle Physics: Snowmass on the Mississippi (CSS2013): Minneapolis, MN, USA, July 29-August 6, 2013* (2013) arXiv:1311.0029 [hep-ph].
  - [5] S. Alekhin *et al.*, Rept. Prog. Phys. **79**, 124201 (2016), arXiv:1504.04855 [hep-ph].
  - [6] D. Notzold and G. Raffelt, Nucl. Phys. **B307**, 924 (1988).
  - [7] L. Wolfenstein, Phys. Rev. **D17**, 2369 (1978).
  - [8] S. P. Mikheev and A. Yu. Smirnov, Sov. J. Nucl. Phys. **42**, 913 (1985), [Yad. Fiz.42,1441(1985)].
  - [9] K. Kainulainen, J. Maalampi, and J. T. Peltoniemi, Nucl. Phys. **B358**, 435 (1991).
  - [10] G. Raffelt and G. Sigl, Astropart. Phys. **1**, 165 (1993), arXiv:astro-ph/9209005 [astro-ph].
  - [11] J. T. Peltoniemi, A&A **254**, 121 (1992).
  - [12] X. Shi and G. Sigl, Phys. Lett. **B323**, 360 (1994), [Erratum: Phys. Lett.B324,516(1994)], arXiv:hep-ph/9312247 [hep-ph].
  - [13] A. Kusenko and G. Segre, Phys. Lett. **B396**, 197 (1997), arXiv:hep-ph/9701311 [hep-ph].
  - [14] A. D. Dolgov, S. H. Hansen, G. Raffelt, and D. V. Semikoz, Nucl. Phys. **B580**, 331 (2000), arXiv:hep-ph/0002223 [hep-ph].
  - [15] A. D. Dolgov and S. H. Hansen, Astropart. Phys. **16**, 339 (2002), arXiv:hep-ph/0009083 [hep-ph].
  - [16] A. D. Dolgov, S. H. Hansen, G. Raffelt, and D. V. Semikoz, Nucl. Phys. **B590**, 562 (2000), arXiv:hep-ph/0008138 [hep-ph].
  - [17] K. Abazajian, G. M. Fuller, and M. Patel, Phys. Rev. **D64**, 023501 (2001), arXiv:astro-ph/0101524 [astro-ph].
  - [18] G. M. Fuller, A. Kusenko, I. Mocioiu, and S. Pascoli, Phys. Rev. **D68**, 103002 (2003), arXiv:astro-ph/0307267 [astro-ph].
  - [19] M. Barkovich, J. C. D'Olivo, and R. Montemayor, Phys. Rev. **D70**, 043005 (2004), arXiv:hep-ph/0402259 [hep-ph].

- [20] J. Hidaka and G. M. Fuller, Phys. Rev. **D74**, 125015 (2006), arXiv:astro-ph/0609425 [astro-ph].
- [21] J. Hidaka and G. M. Fuller, Phys. Rev. **D76**, 083516 (2007), arXiv:0706.3886 [astro-ph].
- [22] A. Kusenko, B. P. Mandal, and A. Mukherjee, Phys. Rev. **D77**, 123009 (2008), arXiv:0801.4734 [astro-ph].
- [23] G. M. Fuller, A. Kusenko, and K. Petraki, Phys. Lett. **B670**, 281 (2009), arXiv:0806.4273 [astro-ph].
- [24] G. G. Raffelt and S. Zhou, Phys. Rev. **D83**, 093014 (2011), arXiv:1102.5124 [hep-ph].
- [25] M.-R. Wu, T. Fischer, L. Huther, G. Martínez-Pinedo, and Y.-Z. Qian, Phys. Rev. **D89**, 061303 (2014), arXiv:1305.2382 [astro-ph.HE].
- [26] M. L. Warren, M. Meixner, G. Mathews, J. Hidaka, and T. Kajino, Phys. Rev. **D90**, 103007 (2014), arXiv:1405.6101 [astro-ph.HE].
- [27] M. Warren, G. J. Mathews, M. Meixner, J. Hidaka, and T. Kajino, Int. J. Mod. Phys. **A31**, 1650137 (2016), arXiv:1603.05503 [astro-ph.HE].
- [28] T. Rembiasz, M. Obergaulinger, M. Masip, M. A. Pérez-Garcia, M.-A. Aloy, and C. Albertus, Phys. Rev. **D98**, 103010 (2018), arXiv:1806.03300 [astro-ph.HE].
- [29] S. Zhou, *Proceedings, International Conference on Massive Neutrinos: Flavor Mixing of Leptons and Neutrino Oscillations: Singapore, Singapore, February 9-13, 2015*, Int. J. Mod. Phys. **A30**, 1530033 (2015), [Adv. Ser. Direct. High Energy Phys.25,243(2015)], arXiv:1504.02729 [hep-ph].
- [30] C. A. Argüelles, V. Brdar, and J. Kopp, Phys. Rev. **D99**, 043012 (2019), arXiv:1605.00654 [hep-ph].
- [31] A. M. Suliga, I. Tamborra, and M.-R. Wu, (2019), arXiv:1908.11382 [astro-ph.HE].
- [32] L. Stodolsky, Phys. Rev. D **36**, 2273 (1987).
- [33] A. Boyarsky, O. Ruchayskiy, D. Iakubovskiy, and J. Franse, Phys. Rev. Lett. **113**, 251301 (2014), arXiv:1402.4119 [astro-ph.CO].
- [34] E. Bulbul, M. Markevitch, A. Foster, R. K. Smith, M. Loewenstein, and S. W. Randall, Astrophys. J. **789**, 13 (2014), arXiv:1402.2301 [astro-ph.CO].
- [35] R. Bollig, H. T. Janka, A. Lohs, G. Martinez-Pinedo, C. J. Horowitz, and T. Melson, Phys. Rev. Lett. **119**, 242702 (2017), arXiv:1706.04630 [astro-ph.HE].
- [36] S. Dodelson and L. M. Widrow, Phys. Rev. Lett. **72**, 17 (1994), arXiv:hep-ph/9303287 [hep-ph].
- [37] X.-D. Shi and G. M. Fuller, Phys. Rev. Lett. **82**, 2832 (1999), arXiv:astro-ph/9810076 [astro-ph].
- [38] T. Asaka, M. Laine, and M. Shaposhnikov, JHEP **01**, 091 (2007), [Erratum: JHEP02,028(2015)], arXiv:hep-ph/0612182 [hep-ph].
- [39] A. Boyarsky, M. Drewes, T. Lasserre, S. Mertens, and O. Ruchayskiy, Prog. Part. Nucl. Phys. **104**, 1 (2019), arXiv:1807.07938 [hep-ph].
- [40] T. Asaka and M. Shaposhnikov, Phys. Lett. **B620**, 17 (2005), arXiv:hep-ph/0505013 [hep-ph].
- [41] T. Asaka, S. Blanchet, and M. Shaposhnikov, Phys. Lett. **B631**, 151 (2005), arXiv:hep-ph/0503065 [hep-ph].
- [42] A. Boyarsky, O. Ruchayskiy, and M. Shaposhnikov, Ann. Rev. Nucl. Part. Sci. **59**, 191 (2009), arXiv:0901.0011 [hep-ph].
- [43] M. Shaposhnikov, JHEP **08**, 008 (2008), arXiv:0804.4542 [hep-ph].
- [44] J. Ghiglieri and M. Laine, JHEP **11**, 171 (2015), arXiv:1506.06752 [hep-ph].
- [45] H. Nunokawa, J. T. Peltoniemi, A. Rossi, and J. W. F. Valle, Phys. Rev. **D56**, 1704 (1997), arXiv:hep-ph/9702372 [hep-ph].
- [46] I. Tamborra, G. G. Raffelt, L. Hudepohl, and H.-T. Janka, JCAP **1201**, 013 (2012), arXiv:1110.2104 [astro-ph.SR].
- [47] Z. Xiong, M.-R. Wu, and Y.-Z. Qian, ApJ **880**, 81 (2019), arXiv:1904.09371 [astro-ph.HE].
- [48] R. Adhikari *et al.*, JCAP **1701**, 025 (2017), arXiv:1602.04816 [hep-ph].
- [49] D. Alp *et al.*, Astrophys. J. **864**, 174 (2018), arXiv:1805.04526 [astro-ph.HE].
- [50] P. Esposito, N. Rea, D. Lazzati, M. Matsuura, R. Perna, and J. A. Pons, Astrophys. J. **857**, 58 (2018), arXiv:1803.04692 [astro-ph.HE].
- [51] J. M. Lattimer and M. Prakash, Astrophys. J. **550**, 426 (2001), arXiv:astro-ph/0002232 [astro-ph].
- [52] J. M. Lattimer, *Proceedings, 33rd SLAC Summer Institute on Particle Physics: Gravity in the Quantum World and the Cosmos (SSI 2005): Menlo Park, California, July 25-August 5, 2005*, eConf **C0507252**, L007 (2005).
- [53] H.-T. Janka, “Neutrino Emission from Supernovae,” in *Handbook of Supernovae*, edited by A. W. Alsabti and P. Murdin (Springer International Publishing AG, 2017) p. 1575, arXiv:1702.08713 [astro-ph.HE].
- [54] G. E. Brown, S. W. Bruenn, and J. C. Wheeler, Comments on Astrophysics **16**, 153 (1992).
- [55] J. F. Beacom, R. N. Boyd, and A. Mezzacappa, Phys. Rev. **D63**, 073011 (2001), arXiv:astro-ph/0010398 [astro-ph].
- [56] K. Blum and D. Kushnir, Astrophys. J. **828**, 31 (2016), arXiv:1601.03422 [astro-ph.HE].
- [57] N. Bar, K. Blum, and G. D’Amico, (2019), arXiv:1907.05020 [hep-ph].
- [58] A. Burrows, M. S. Turner, and R. P. Brinkmann, Phys. Rev. **D39**, 1020 (1989).
- [59] W. Keil, H.-T. Janka, D. N. Schramm, G. Sigl, M. S. Turner, and J. R. Ellis, Phys. Rev. **D56**, 2419 (1997), arXiv:astro-ph/9612222 [astro-ph].
- [60] T. Fischer, S. Chakraborty, M. Giannotti, A. Mirizzi, A. Payez, and A. Ringwald, Phys. Rev. **D94**, 085012 (2016), arXiv:1605.08780 [astro-ph.HE].
- [61] S. J. Parke, *Proceedings, 23RD International Conference on High Energy Physics, JULY 16-23, 1986, Berkeley, CA*, Phys. Rev. Lett. **57**, 1275 (1986).
- [62] J. Bliss, M. Witt, A. Arcones, F. Montes, and J. Pereira, Astrophys. J. **855**, 135 (2018), arXiv:1802.00737 [astro-ph.HE].
- [63] T. A. Thompson, A. Burrows, and J. E. Horvath, Phys. Rev. **C62**, 035802 (2000), arXiv:astro-ph/0003054 [astro-ph].